Gas-Liquid Flow through Horizontal Tees of Branching and Impacting Type

Dimitri Hatziavramidis
Mobil E&P Technical Center, Dallas, TX 75381

Bing Sun and Dimitri Gidaspow
Dept. of Chemical Engineering, Illinois Institute of Technology, Chicago, IL 60616

In gas–liquid flows through tee junctions, because of the difference in inertia between the phases, the flowing mass fractions for an individual phase at the outlet sides differ from those at the inlet. This phase separation is an important consideration in delivering fluids and energy through pipe networks in the power and process industry. In this work, air–water and steam–water flows through branching and impacting tee junctions are considered. Under certain conditions (when the volumetric fraction of the liquid drops does not change appreciably and their bulk density is much higher than the gas density, and when the flow rates and/or the gas volumetric fraction are high), these flows can be approximated as irrotational flows of incompressible, inviscid fluids and are amenable to potential flow methods, for example, conformal mapping. For the general case of gas–liquid flows through a branching or impacting tee, a CFD code is utilized to conduct transient flow simulations. Predictions of phase separation for both types of tee junction agree well with experimental data.

Introduction

Tee junctions are common features of single-phase and two-phase flow-distribution systems in the power and process industries. In gas–liquid flows through tee junctions, the phases, because of their difference in inertia, are accelerated differently and the flowing mass fractions at the outlet sides are different from those at the inlet. This phase separation is of major importance to many applications, including but not limited to oil recovery. In thermal oil recovery, distribution of steam from the generator to the steam-injecting wells opts for controlled rate and high quality of steam delivered to the individual wells so that a better distribution of heat to the oil field, and thus, higher oil recovery is achieved.

Phase separation in flows through tee junctions has been a subject of numerous investigations, experimental and theoretical (Fouda and Rhodes, 1972; Hong, 1978; Azzopardi and Whalley, 1982; Saba and Lahey, 1984; Seeger et al., 1986; Smoglie and Reimann, 1986; Shoham et al., 1987; Hwang et al., 1988, 1989; Azzopardi et al., 1987; Rubel et al., 1988; Ballyk and Shoukri, 1990; McCreery and Banerjee, 1990; Kimpland et al., 1992; Buell et al., 1994; Kalkach-Navarro et al., 1995, etc.). According to these investigations, phase separation in a tee junction is affected by (1) the type, that is, branching or impacting (Figure 1), and the orientations, for example, numerous combinations of horizontal, upward and downward inlet and outlet sides of the tee; (2) the inlet flow pattern, for example, stratified, annular, dispersed; (3) the inlet flow rate; (4) inlet pressure; (5) inlet quality; (6) diameters of the inlet and outlet sides, and so on.

Much of the earlier work on gas–liquid flows through tee junctions relies on empirical and phenomenological models. The empirical models (Seeger et al., 1986) correlate experimental data in terms of outlet-to-inlet quality and flow-rate ratios. The phenomenological models (Hwang et al., 1988) utilize the one-dimensional flow equations and the concept of "dividing streamlines" or "zones of influence."

The work presented here employs two approaches to model gas–liquid flows through a tee junction: (1) a conformal mapping technique, and (2) CFD transient flow simulations. A comparison of predictions by both approaches confirms that

Present address of D. Hatziavramidis: GE Plastics, 1 Lexan Lane, Mt. Vernon, IN 47620.

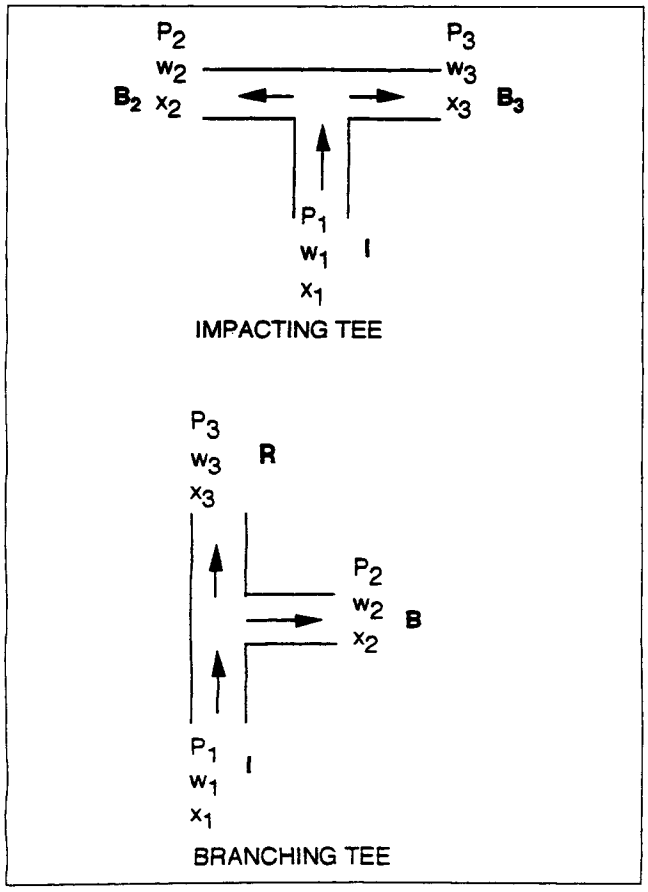

Figure 1. Flow through tee junctions.

the conformal mapping technique generates a good approximation to certain types of gas–liquid flows. The predictions of flow patterns and phase separation by the CFD simulations are shown to be in good agreement with experimental data.

Conformal Mapping for Gas-Liquid Flows

The use of conformal mapping for certain types of two-dimensional single-phase flows, for example, potential flows (i.e., irrotational flows of incompressible and inviscid fluids) and slow viscous flows (e.g., Hele-Shaw flows and flows through porous media), has been well documented (Lamb, 1945; Scheidegger, 1960). Applications of conformal mapping to two-phase flows, particularly in the area of fluidization, have also been reported (Davidson and Harrison, 1963; Gidaspow, 1994).

In a gas–liquid flow, when the volume fraction of the liquid droplets does not change appreciably and the droplet bulk density is much larger than the gas density, the vorticity of the droplets remains constant along their streamlines (Gidaspow, 1994), thus rendering the flow irrotational. When the flow rate is high, as is the case with turbulent shear flows, and/or the gas volumetric fraction is high, inertia forces dominate viscous forces, and the fluid system can be approximated as inviscid. In view of the irrotational, incompressible, and inviscid approximations, this type of gas–liquid flow is amenable to potential flow analysis.

In this article, conformal mapping is applied to gas–liquid flows through horizontal tees, for which the potential flow approximation can be made. Conformal mapping is applied here not in its conventional form, which would have resulted in infinite velocities at the sharp corners on the boundary, but in a form appropriate to flow separation at sharp corners, which assures finite velocities there (Copson, 1961). The streamline that defines the boundary of flow separation is called a free streamline, and in single-phase flow separates the fluid in motion from the fluid at rest. As comparison with the numerical results will show later, the free streamline in this work separates the faster, "more inviscid" fluid from the slower, "less inviscid" fluid.

The width of the conduit, L, approximates the diameter of the pipe, which, in the work presented here is the same for inlet and outlet sides. The complex velocity for this two-dimensional potential flow

$$\upsilon = \upsilon_x + i\upsilon_y \tag{1}$$

is related to the velocity potential Φ and the stream function Ψ through

$$\upsilon_x = \Phi_x = \Psi_y \tag{2a}$$

$$\upsilon_y = \Phi_y = -\Psi_x. \tag{2b}$$

The original flow z-plane is transformed as shown in Figures 2 and 3 into Q-plane, Ψ-plane, and λ-plane, successively, using the Schwarz–Christoffel transformation.

The analytic function Q is defined from the complex potential w by

$$Q = \ln V_{sb} - \ln \frac{dw}{dz} = \ln\left(\frac{V_{sb}}{|V|}\right) + i\theta, \tag{3}$$

where V_{sb} is the superficial flow velocity in the branch and $|V| = (\upsilon_x + \upsilon_y)^{1/2}$.

The flow plane contains a free streamline and stagnation points at which the velocity is required to vanish.

Branching tee junction

The z-plane for the branching tee junction, which contains a stagnation point $S = B$ and the free streamline $A - C_R$, is shown in Figure 2. The thickness of the stagnant fluid region is $L_{x\infty}$, and thus fluid flows only in the area between the free streamline and the pipe wall $B - C_L$.

The transformation from the Q- and the λ-plane (Figure 2) reads

$$\frac{dQ}{d\lambda} = \frac{K}{(\lambda+1)^{1/2}\lambda^{1/2}}. \tag{4}$$

Integration of 4 yields

$$Q = 2K \ln(\sqrt{\lambda+1} + \sqrt{\lambda}) + C \tag{5}$$

and the constants K and C are determined from the boundary conditions: point $C \rightarrow \lambda = 0$ and $Q = i\pi/2$; point $A \rightarrow \lambda$

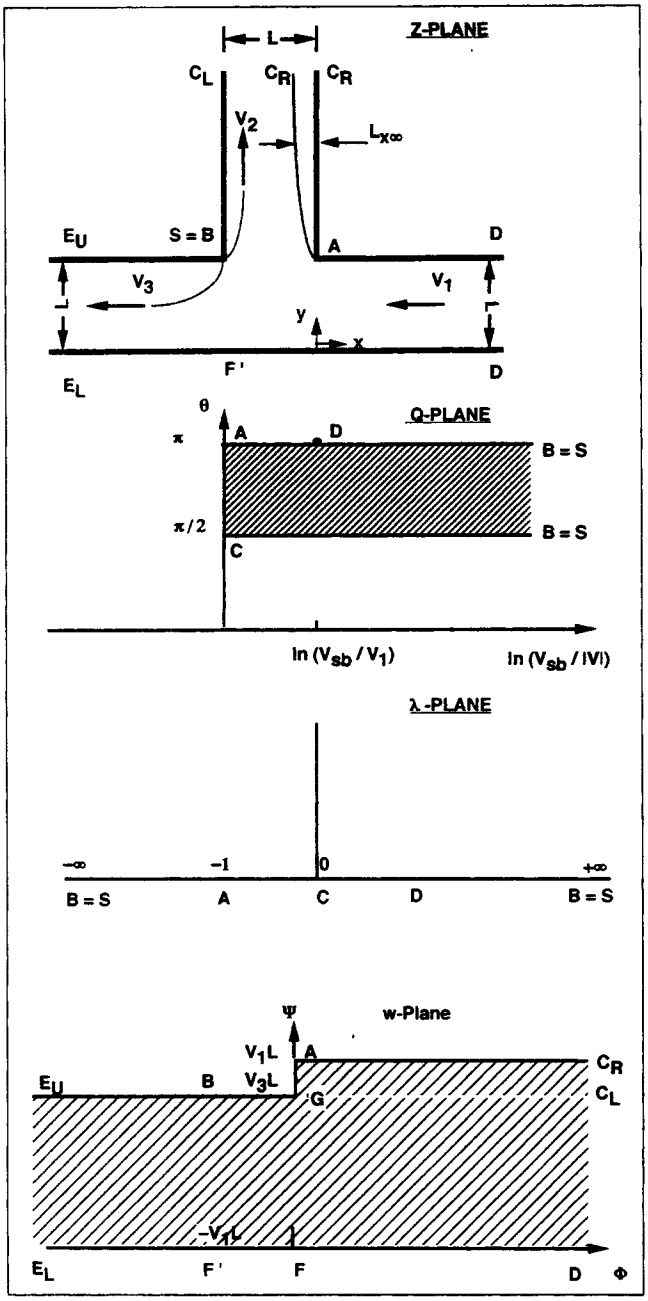

Figure 2. Conformal mapping transformations for flow through a branching tee.

$= -1$ and $Q = i\pi$. In view of this, the expression for Q becomes

$$Q = \ln[i(\sqrt{\lambda+1} + \sqrt{\lambda})]. \tag{6}$$

The transformation from the w- to the λ-plane (Figure 2) reads

$$\frac{dw}{d\lambda} = \frac{K'}{(\lambda-1)^{1/2}(\lambda+1)^{1/2}} \tag{7}$$

which, after integration, becomes

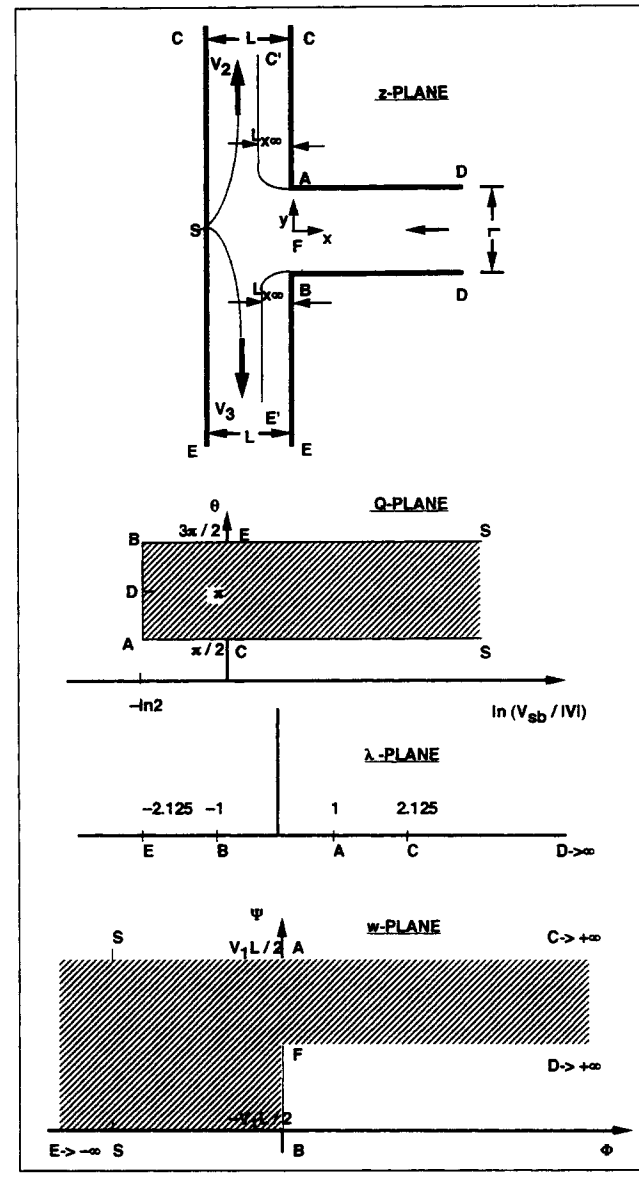

Figure 3. Conformal mapping transformations for flow through an impacting tee.

$$w = 2K' \ln(\sqrt{\lambda-1} + \sqrt{\lambda+1}) + C'. \tag{8}$$

With the boundary conditions, $A \to \lambda = -1$, $w = iV_1L$; $G \to \lambda = +1$, $w = iV_3L$, the constants of Eq. 8 are determined to be

$$K' = (V_1 - V_3)\frac{L}{\pi}; \quad C' = \left[iV_3 - \frac{\ln 2}{\pi}(V_1 - V_3)\right]L.$$

Since

$$Q = \ln\left[(V_1 - V_3)\frac{dz}{dw}\right] = \ln\left[V_{sb}\frac{dz}{dw}\right], \tag{9}$$

from Eqs. 6 and 9

$$V_{sb}\frac{dz}{dw} = i(\sqrt{\lambda+1}+\sqrt{\lambda}). \tag{10}$$

From Eqs. 7 and 10

$$\frac{dz}{d\lambda} = \frac{iK'}{V_{sb}}\frac{(\sqrt{\lambda+1}+\sqrt{\lambda})}{\sqrt{\lambda^2-1}}. \tag{11}$$

Equation 11, which defines the free streamline $A-C_R$, after integrating between A and C_R, yields (Prudnikov et al., 1987)

$$x+iy-iL = \int_{-1}^{\lambda}\frac{iK'}{V_{sb}}\frac{(\sqrt{\lambda+1}+\sqrt{\lambda})}{\sqrt{\lambda^2-1}}d\lambda$$

$$= \frac{iK'}{V_{sb}}[2(i\sqrt{1-\lambda}-\sqrt{2})+\sqrt{2}(2E(\varphi,k)-F(\varphi,k))], \tag{12}$$

where $E(.)$ and $F(.)$ are elliptic integrals and

$$\varphi = \arcsin(\sqrt{\lambda+1}); \quad k = \frac{\sqrt{2}}{2}. \tag{13}$$

For $\lambda \to 0$, Eq. 12 yields

$$x = -0.637L; \quad y = 1.481L,$$

which means that, after $y > 1.481L$, the distance of the free streamline from the underlying pipe wall is constant and equal to $0.637L$. Hence, the flow in the branch is limited to a cross section of width $0.363L$.

Impacting tee junction

The flow plane for the impacting tee contains the stagnation point S and the free streamline AC' (Figure 3).

The transformation between the Q-plane and λ-plane (Figure 3) is

$$\frac{dQ}{d\lambda} = \frac{K}{\sqrt{\lambda^2-1}}, \tag{14}$$

which, after integration, and with the boundary conditions set at points A ($\lambda=1$, $Q=i\pi/2$) and B($\lambda=-1$, $Q=i3\pi/2$), yields

$$Q = \ln\left(i\frac{\sqrt{\lambda-1}+\sqrt{\lambda+1}}{2\sqrt{2}}\right) \tag{15}$$

From Eq. 15 one obtains

$$V_{sb}\frac{dz}{dw} = \frac{1}{2\sqrt{\lambda^2-1}}. \tag{16}$$

The transformation between the w-plane and λ-plane (Figure 3) is

$$\frac{dw}{d\lambda} = \frac{K'}{\sqrt{\lambda(\lambda+1)}}. \tag{17}$$

Integrating (Eq. 17) and applying the boundary conditions at B ($\lambda=-1$, $w=-iV_1L/2$) and F ($\lambda=0$, $w=0$), we get $K' = -V_1L/2\pi$ and

$$w = -\frac{V_1L}{\pi}\ln(\sqrt{\lambda+1}\sqrt{\lambda}). \tag{18}$$

From Eqs. 16 and 17, one obtains

$$\frac{dz}{d\lambda} = -\frac{iL}{2\sqrt{2}\pi}\frac{(\sqrt{\lambda+1}+\sqrt{\lambda-1})}{\sqrt{\lambda(\lambda+1)}}. \tag{19}$$

This is the equation for the free streamline, which, after integrating from B ($\lambda=-1$) to E ($\lambda=-2.125$) becomes

$$x+iy-\left(-\frac{iL}{2}\right) = -\frac{iL}{2\sqrt{2}\pi}\left\{-2i\left[\sqrt{2}(F-E)(\varphi,k) + \sqrt{\frac{\lambda^2-1}{-\lambda}}\right]+2i(\sqrt{\lambda}-1)\right\}, \tag{20}$$

where $\varphi = \arcsin[(1+\lambda)/\lambda]^{1/2}$ and $k = 2^{1/2}/2$. Equation 20, for $\lambda=-2.125$ (which corresponds to point E), yields

$$x = -\frac{1.892L}{2\sqrt{2}\pi} \approx -0.213L; \quad y = -0.5L.$$

Thus, for an impacting tee junction, from the corner on, the flow in the branches is limited to a cross section with dimension $0.787L$.

Computations of Gas-Liquid Flows Through Tee Junctions

A hydrodynamic code, based on the Los Alamos code K-FIX, and modified over the years at the Illinois Institute of Technology (IIT), was used to conduct simulations of two-dimensional, gas–liquid flows through tee junctions (Sun, 1996). This code solves the two-dimensional mass and momentum balance equations for each phase,

$$\frac{\partial}{\partial t}(\alpha_k\rho_k)+\nabla\cdot(\alpha_k\rho_k\mathbf{u}_k)=0 \quad k=g \text{ or } l \tag{21}$$

$$\frac{\partial}{\partial t}(\alpha_g\rho_g\mathbf{u}_g)+\nabla\cdot(\alpha_g\rho_g\mathbf{u}_g\mathbf{u}_g) = -\nabla p+\rho_g\mathbf{g}+\nabla\cdot\boldsymbol{\tau}_g+\beta(\mathbf{u}_l-\mathbf{u}_g) \tag{22}$$

$$\frac{\partial}{\partial t}(\alpha_l\rho_l\mathbf{u}_l)+\nabla\cdot(\alpha_l\rho_l\mathbf{u}_l\mathbf{u}_l) = \alpha_l(\rho_l-\rho_g)\mathbf{g}+\nabla\cdot\boldsymbol{\tau}_l+\beta(\mathbf{u}_g-\mathbf{u}_l). \tag{23}$$

In the preceding equations, α_k, ρ_k, and $\boldsymbol{u}_k$, $k = g$ or l, are the volumetric fraction, density, and velocity (vector) of the k-phase, respectively, and p is the pressure. The fluid stress, $\boldsymbol{\tau}_k$, is given by

$$\boldsymbol{\tau}_k = \alpha_k \mu_{kc}\left[\nabla \boldsymbol{u}_k + (\nabla \boldsymbol{u}_k)^T\right] - \frac{2}{3}\alpha_k \mu_{kc} \nabla \cdot \boldsymbol{u}_k \boldsymbol{I}, \quad (24)$$

where μ_{kc} is the viscosity of the gas ($k = g$) or the liquid ($k = 1$).

The interfacial drag coefficient is

$$\beta = 150\frac{\alpha_l^2 \mu_g}{(\alpha_g d_p)^2} + 1.75\frac{\rho_g \alpha_l |\boldsymbol{u}_g - \boldsymbol{u}_l|}{\alpha_g d_p} \quad \text{for} \quad \alpha_g < 0.8$$

$$= \frac{3}{4} c_D \frac{\rho_g \alpha_l |\boldsymbol{u}_g - \boldsymbol{u}_l|}{d_p} \alpha_g^{-2.65} \quad \text{for} \quad \alpha_g \geq 0.8, \quad (25)$$

with d_p being the droplet diameter, c_D, the drag coefficient, given by

$$c_D = \frac{24}{Re}[1 + 0.15\, Re^{0.687}] \quad Re < 1{,}000$$

$$= 0.44 \quad Re \geq 1{,}000 \quad (26)$$

and the Reynolds number defined as

$$Re = \frac{\alpha_g \rho_g |\boldsymbol{u}_g - \boldsymbol{u}_l| d_p}{\mu_g}. \quad (27)$$

The expression for interfacial drag used here do not require a certain distribution of gas and liquid, that is, a flow regime (stratified, annular, etc.), to be assumed. Instead, the distribution of the fluids (flow regime) results from the numerical solution.

Equations 21–23 together with the constitutive equation, Eq. 24, the expressions for the interfacial drag, Eqs. 25–27, and the equation of state for the gas, are solved in terms of the velocity components, u_x and u_y, for each phase, the void fraction, α, and the pressure, p.

The equations are discretized, using the implicit continuous Eulerian (ICE) method (Rivard and Torrey, 1977), on a staggered grid with scalar variables (e.g., pressure) defined at the gridblock center and vector variables (e.g, velocity) defined at gridblock boundaries. Fluxes are differenced using the conservative "donor-cell" (or second upwind differencing) scheme and are explicit in time, whereas all exchanges of mass and momentum between the phases are treated implicitly. The resulting finite difference equations are solved by a combination of Newton's and secant methods, without linearization.

The two-fluid formulation has been shown to lead to an ill-posed initial-value problem, in the sense it possesses imaginary characteristics. Gidaspow (1986) proposed several ways to cure the ill-posedness problem, including but not limited to deriving a relative-velocity equation using nonequilibrium thermodynamics. Because of the usually small numerical values of the imaginary characteristics and the comparatively large numerical dumping, K-FIX and its successors were able to produce at times reasonable results.

Branching tee simulations

The two-dimensional grid utilized for branching tee simulations is shown in Figure 4 in a double-logarithmic, double-ordinate plot. Unequal gridblocks, with the greatest linear dimension being 21 cm and the smallest 0.3 cm, are utilized with a closer spacing in the proximity of the boundaries and the flow turn. In all, 51 gridblocks in the x-direction and 39 gridblocks in the z-direction are used. Figure 4 shows that sufficiently long straight-pipe sections upstream and downstream of the junction were utilized in the simulations. Due to stability requirements, the time step was 2×10^{-5} s. However, the system reached steady state in less than a minute.

Regarding the boundary conditions, the inlet flow to the branching tee is specified to be homogeneous, dispersed. The discharge pressure for the branch and run outlets are also specified (Sun, 1996) in accordance with the mass-flux ratios in the experiments of Seeger et al. (1986).

The results of the two-phase flow simulations for the branching tee, using IIT's hydrodynamic code, are compared to the experimental data of Seeger et al. (1986).

Figure 5 shows simulation and experimental results in terms of mass-flux ratio, G_3/G_1, vs. gas mass fraction or quality ratios, x_3/x_1, where the subscript 1 and 3 stand for the main pipe and the branch, respectively, for air–water flowing in a horizontal branching tee with unchanged diameter of 5.5 cm, at inlet pressure of 0.7 MPa and superficial velocities 1 m/s for the liquid and 10 m/s for the gas. In the same figure, equal separation and total-phase separation curves and a best-fit curve of the experiments are shown. A comparison of simulations to experiments show them to be in good agreement. At high mass-flux ratios, G_3/G_1, phase separation approaches the total separation curve. In the vicinity of $G_3/G_1 = 0.3$, phase separation reaches a maximum. Limited results show that, as the gas superficial velocity increases, which corresponds to increasing the gas momentum flux, phase separation decreases.

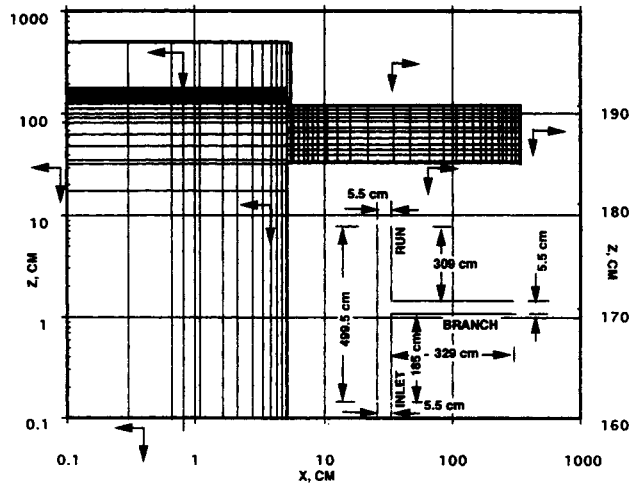

Figure 4. Computational grid for branching tee simulations.

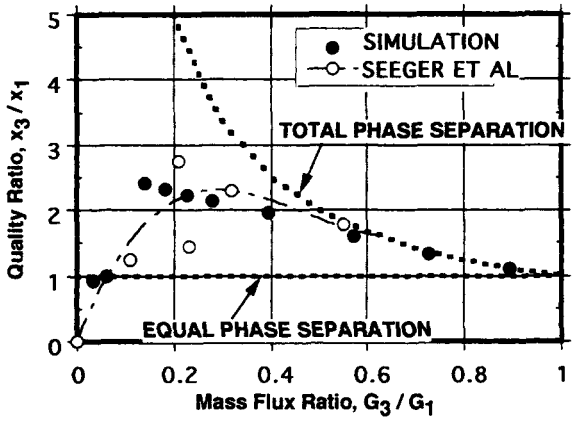

Figure 5. Phase separation from experiments and simulations of air/water flows through a branching tee.

Inlet pressure 0.7 MPa; superficial velocities, gas: 10 m/s, liquid: 1 m/s.

The experiments of Seeger et al. (1986) start at mass-flux ratios greater than 0.10 and, as the authors argue, "the point $x_3/x_1 = 0$ and $G_3/G_1 = 0$ is pure speculative." In the vicinity of a mass-flux ratio of 0.1, the authors have found that the experimental error is $\pm 40\%$. The simulations, on the other hand, cover the entire mass-flux ratio range from 0 to 1. For mass-flux ratios greater than 0.1, the drop size was selected to be 0.01 cm; for ratios less than 0.1, the drop size was reduced to 0.0001 cm and the grid was further refined.

The majority of the air–water flows in the experiments of Seeger et al. (1986) had a high gas volumetric fraction, approximately 0.90. From visualizations of the simulation results for air–water simulations, after steady state, the following flow patterns emerged. A thin liquid film coats the walls of the main pipe, rendering the flow annular with most of the liquid in the dispersed phase. In the branch, most of the liquid and gas flow along the downstream wall; the rest of the fluid along the upstream wall is, for all practical purposes, stagnant (the velocity is very small or slightly reversed). A vector plot of the liquid velocities from simulations of the experiments by Seeger et al. (1986) at inlet pressure 0.7 MPa, superficial liquid and gas velocities of 1 and 10 m/s, respectively, and mass-flux ratio 0.2787, is shown in Figure 6. In the branch, the liquid flows in the upper one-third of the channel width where the majority of the gas also flows. This agrees with the potential flow solution in the conformal mapping section, which shows that the flow in the branch is confined to the upper 36% of the channel width, while the lower 64% of the channel width is occupied by stagnant fluid.

Figure 7 shows simulation and experimental results in terms of phase separation for air–water and steam–water flowing in a horizontal branching tee with unchanged diameter of 5.5 cm, at inlet pressures of 0.4, 1, and 2.5 MPa. In the same figure, the equal and total-phase separation curves and the best-fit to experimental data at 2.5 MPa curves are shown. Again, the agreement of the air–water and steam–water simulations and experiments in the horizontal branching tee is remarkable. As expected, as the inlet pressure increases, which corresponds again to increasing the gas-momentum flux, phase separation decreases.

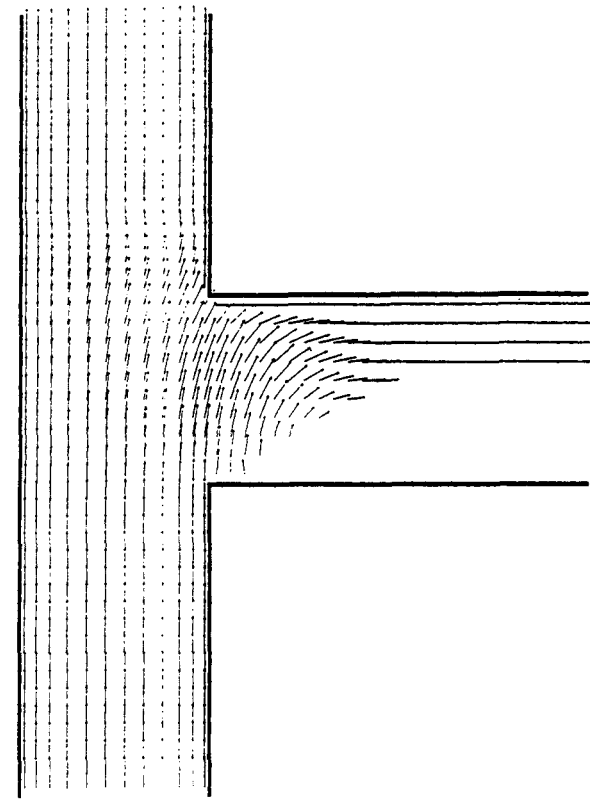

Figure 6. Liquid-velocity distribution from simulations of air/water flow through a branching tee.

Inlet pressure, 0.7 MPa; superficial velocities, gas: 10 m/s, liquid: 1 m/s; mass flux ratio, 0.2787.

Impacting tee simulations

As with the branching tee, because the radius of the pipes in the junction is much smaller than their lengths, the two-dimensional grid utilized for the impacting tee is nonuniform. Unequal gridblocks with the greatest linear dimension being 16 cm and the smallest 0.38 and 0.508 cm, for air–water and wet steam, respectively, are utilized with a closer spacing in

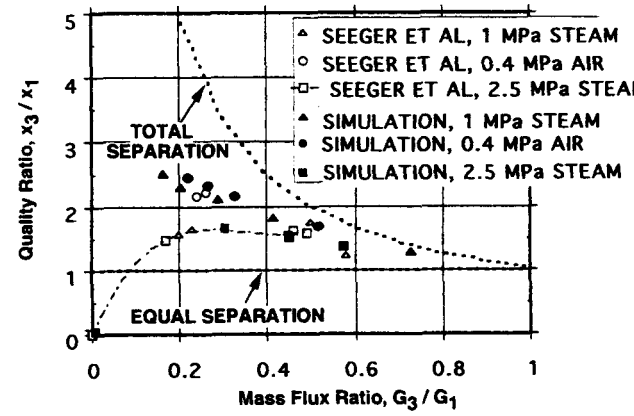

Figure 7. Phase separation from experiments and simulations of air/water and wet stream flows through a branching tee.

Varying inlet pressure; superficial velocities; gas: 10 m/s, liquid: 2 m/s.

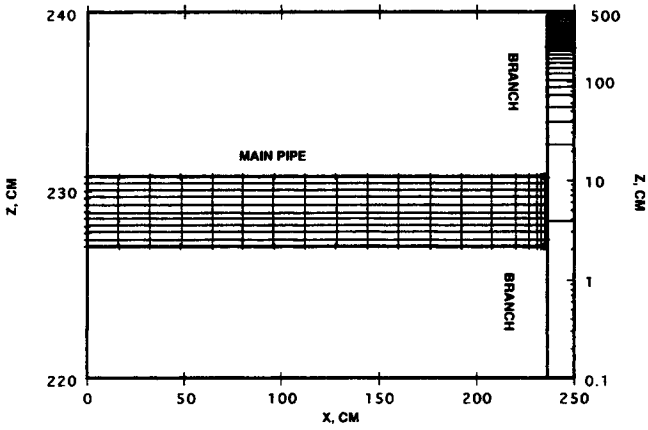

Figure 8. Computational grid for impacting tee simulations.

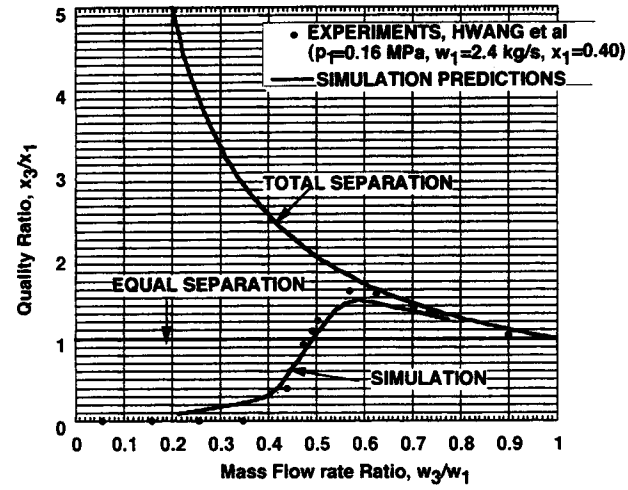

Figure 10. Phase separation from experiments and simulations of air/water flows through an impacting tee.

the proximity of the boundaries and the flow turns. In all, 33 gridblocks in the x-direction and 74 in the z-direction are used, as shown in Figure 8 in a double-logarithmic, double-ordinate plot. Sufficiently long straight-pipe sections upstream and downstream of the junction and flow turns are utilized so that the effects of the boundaries neither downstream (for high-momentum flows, e.g., annular and intermittent) nor upstream (for low-momentum flows, e.g., stratified) influence the flow in the vicinity of the junction. Due to stability requirements, the time step for the impacting tee simulations was 2×10^{-5} s.

Contrary to the branching tee simulations, where the system reached steady state in less than a minute, the transient flow in the impacting tee never reached true steady state. Figure 9 shows the variation with time of the mass flow-rate ratio, w_3/w_1, for air–water in an impacting tee. From this figure, a three-stage development of flow in the impacting tee emerges: (1) a transient stage of gradual change, approxi-

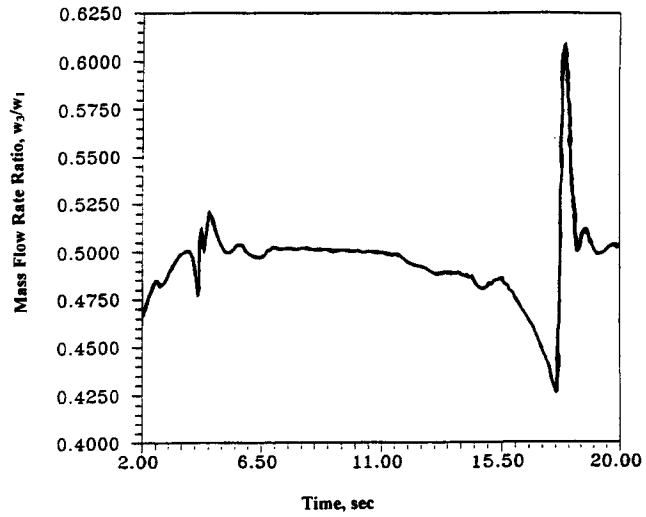

Figure 9. Variation of mass flow-rate ratio with time of simulation of air/water flow through an impacting tee.

Inlet pressure, 0.16 MPa; branch pressures, 0.159 MPa; inlet mass flow rate, 2.40 kg/s; inlet quality, 0.40.

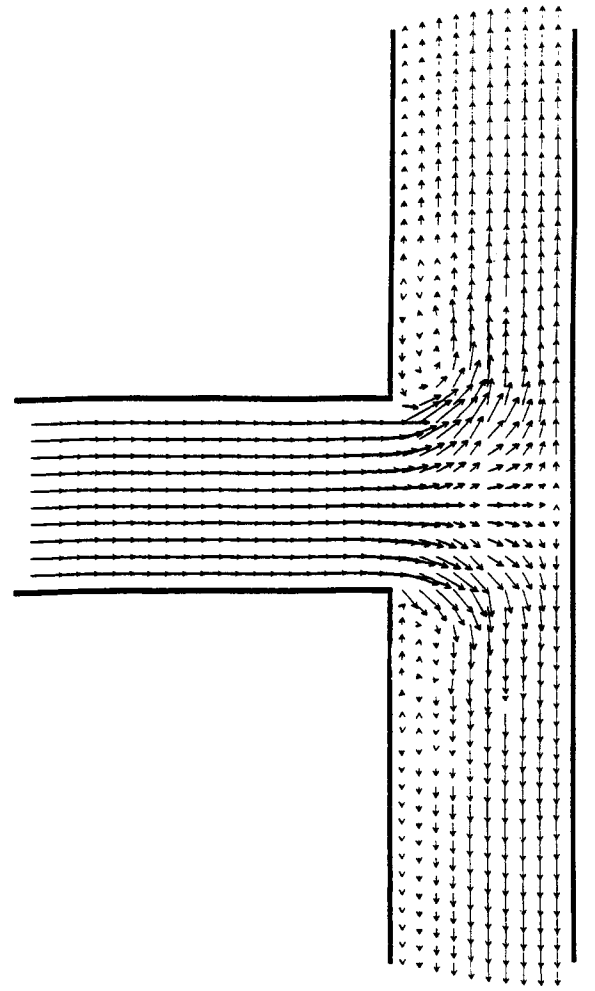

Figure 11. Gas-velocity distribution at 10 s of simulation time for air/water flow through an impacting tee.

Inlet pressure, 400 psig (2.76 MPa); branch pressures, 397.1 psig (2.74 MPa); gas velocity, 40 ft/s (12 m/s); quality, 0.39.

mately 5 s in duration; (2) a relatively steady stage of small fluctuations, approximately 10 s in duration; and (3) a stage of large fluctuations. The unsteady character of the two-phase flow in the impacting tee, under the aforementioned conditions, is directly related to the type of flow regime, slug flow, in this case, which is inherently unstable. Visualizations of the flow of interest at 10 s show that the liquid slug is located in the immediate vicinity of the point of impact.

The simulations of air–water in a horizontal impacting tee with equal and unequal discharge pressures in the branches duplicate experiments conducted by Hwang et al. (1989). Figure 10 shows simulation predictions and experimental data in terms of quality ratio, x/x_1 vs. mass flow-rate ratio, w_3/w_1, for air–water flowing in a horizontal impacting tee with unchanged diameter of 3.8 cm, at inlet pressure of 0.16 MPa, mass flow rates of 2.4 kg/s, and quality 0.40. The agreement of predictions and measurements is excellent. For low mass flow-rate ratios (i.e., < 0.40), small or no amount of gas flows through branch "3." As the mass flow-rate ratio increases, the quality ratio approaches the total separation curve and reaches a peak at approximately 0.50 mass flow-rate ratio.

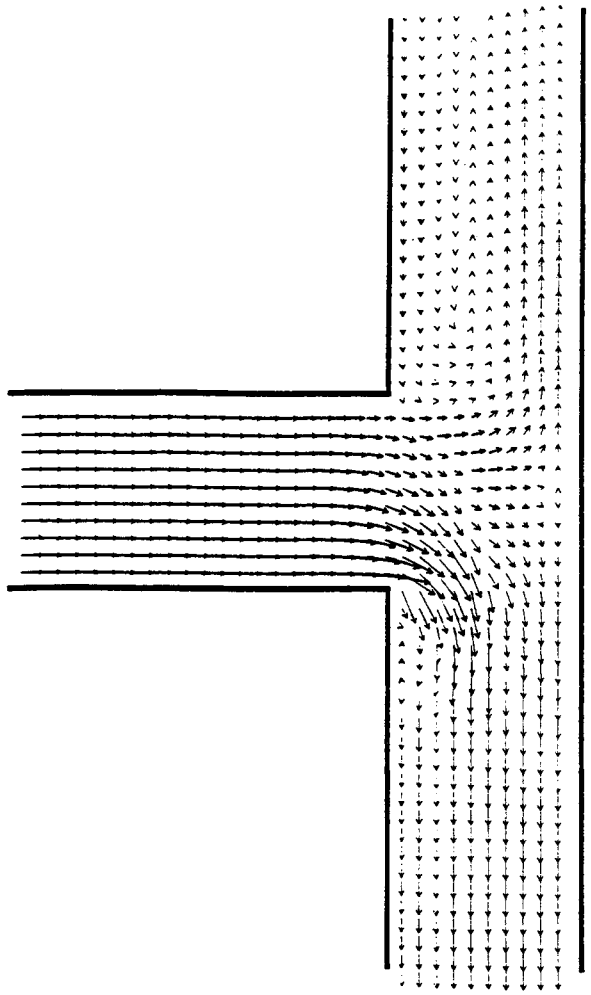

Figure 12. Gas-velocity distribution at 10 s of simulation time for air/water flow through an impacting tee.

Inlet pressure, 400 psig (2.76 MPa); branch pressures, 397.1 and 388.4 psig (2.74 and 2.68 MPa); gas velocity, 40 ft/s (12 m/s), quality, 0.39.

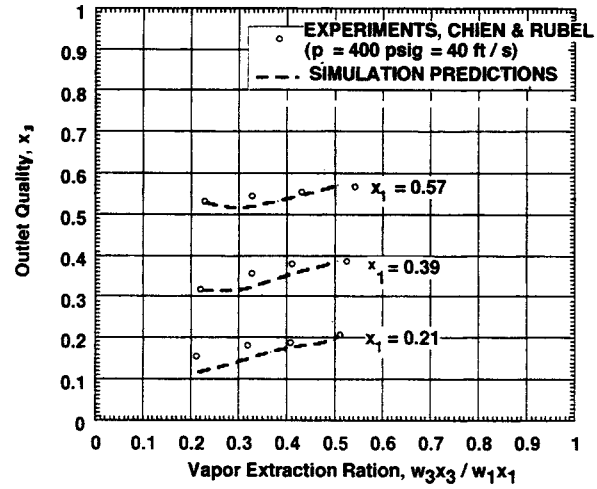

Figure 13. Phase separation from experiments and simulations of wet steam flows through an impacting tee.

Figures 11 and 12 show the vector plot of the gas velocity at 10 s from simulations of air–water flows in the experiments of Hwang et al. (1989), at inlet pressure 0.16 MPa, mass flow-rate 2.40 kg/s, and quality 0.40. With equal discharge pressures of 0.159 MPa in both branches, Figure 11 shows complete symmetry of the flow, as expected. It is also noticeable that in the lower 20% of the channel width in the branches, the velocity of gas is small and, sometimes, slightly reversed. Because the flow rate and gas volumetric fraction of the flows of interest are high, this is in agreement with the potential flow solution of the previous section that predicts that flow occurs in the upper 79% cross-sectional area of the branch. For the exact same system, when unequal discharge pressures in the branches, 0.135 and 0.159 MPa, are imposed, Figure 12 shows that the flow becomes asymmetric with more gas flowing in the low-discharge-pressure branch.

The simulations of wet steam in a horizontal impacting tee with equal and unequal discharge pressures in the branches duplicate experiments conducted by Chien and Rubel (1989). Figure 13 shows simulation and experimental results in terms of outlet quality, x_3, vs. vapor-extraction ratio, w_3x_3/w_1x_1, for wet steam flowing in a horizontal impacting tee with an unchanged diameter of 2 in., at inlet pressure of 400 psig (2.8 MPa), superficial gas velocity of 40 ft/s (12 m/s) and inlet qualities 0.21–0.57. The agreement between predictions and measurements is again noticeable. There is clearly a difference between outlet and inlet quality if the vapor-extraction ratio is different from 0.5. As this ratio deviates further from 0.5, the difference between outlet and inlet quality increases. As the inlet quality increases, this difference decreases.

Literature Cited

Azzopardi, B. J., and P. B. Whalley, "The Effect of Flow Patterns on Two-Phase Flow in a T Junction," *Int. J. Multiphase Flow*, **8**, 491 (1982).

Azzopardi, B. J., A. Purvis, and A. H. Govan, "Annular Two-Phase Flow Split at an Impacting T," *Int. J. Multiphase Flow*, **13**, 605 (1987).

Ballyk, J. D., M. Shoukri, and A. M. C. Chan, "Steam-Water Annular Flow in a Horizontal Dividing T-Junction," *Int. J. Multiphase Flow*, **14**, 265 (1988).

Buell, J. R., H. M. Soliman, and G. E. Sims, "Two-phase Pressure Drop and Phase Distribution at a Horizontal Tee Junction," *Int. J. Multiphase Flow*, **20**, 819 (1994).
Chien, S.-F., and M. T. Rubel, "Phase Splitting on Wet Steam in Annular Flow Through a Horizontal Impacting Tee," *SPE Prod. Eng.*, 368 (1992).
Copson, E. T., *Theory of Functions of a Complex Variable*, Oxford University Press, New York (1961).
Davidson, J. F., and D. Harrison, *Fluidized Particles*, Cambridge University Press, New York (1963).
Fouda, A. E., and E. Rhodes, "Two-Phase Annular Flow Stream Division in Simple Tee," *Trans. Inst. Chem. Eng.*, **52**, 354 (1974).
Gidaspow, D., *Multiphase Flow and Fluidization*, Academic Press, New York (1994).
Gidaspow, D., "Hydrodynamics of Fluidization and Heat Transfer: Supercomputing Modeling," *Appl. Mech. Rev.*, **39**, 3 (1986).
Hong, K. C., "Two-phase Flow Splitting at a Pipe Tee," *J. Pet. Tech.*, 290 (1978).
Hwang, S. T., H. M. Soliman, and R. T. Lahey, "Phase Separation in Dividing Two-phase Flows," *Int. J. Multiphase Flow*, **14**, 439 (1988).
Hwang, S. T., H. M. Soliman, and R. T. Lahey, "Phase Separation in Impacting Wyes and Tees," *Int. J. Multiphase Flow*, **15**, 965 (1989).
Kalkach-Navarro, S., S. J. Lee, R. T. Lahey, and D. A. Drew, "The Prediction of Phase Separation in a Branching Conduit using a Three-Dimensional Two-Fluid Model," *Int. J. Multiphase Flow* (1994).
Kimpland, R. H., R. T. Lahey, B. J. Azzopardi, and H. M. Soliman, "A Contribution to the Prediction of Phase Separation in Branching Conduits," *Chem. Eng. Commun.*, **111**, 79 (1992).
Lamb, H., *Hydrodynamics*, Dover, New York (1945).
McCreery, G. E., and S. Banerjee, "Phase Separation of Dispersed Mist and Dispersed Annular (Rivulet or Thin Film) Flow in a Tee: I. Experiments," *Int. J. Multiphase Flow*, **16**, 429 (1990).
Prudnikov, A. P., Yu. A. Brychkov, and O. I. Marichev, *Integrals and Series*, Gordon & Breach, New York (1987).
Rivard, W. C., and M. D. Torrey, "K-FIX: A Computer Program for Transient, Two-dimensional, Two-fluid Flow," LA-NUREG-6623, Los Alamos Nat. Lab., Los Alamos, NM (1977).
Rubel, M. T., H. M. Soliman, and G. E. Sims, "Phase Distribution during Steam-Water Flow in a Horizontal T-Junction," *Int. J. Multiphase Flow*, **14**, 425 (1988).
Saba, N., and R. T. Lahey, "The Analysis of Phase Separation Phenomena in Branching Conduits," *Int. J. Multiphase Flow*, **10**, 1 (1984).
Scheidegger, A., *The Physics of Flow through Porous Media*, Univ. of Toronto Press, Toronto, Ont., Canada (1960).
Seeger, W., J. Reimann, and U. Muller, "Two-phase Flow in a T-Junction with a Horizontal Inlet—Part I: Phase Separation," *Int. J. Multiphase Flow*, **12**, 575 (1986).
Shoham, O., J. P. Brill, and Y. Taitel, "Two-phase Flow Splitting in a Tee Junction—Experiment and Modeling," *Chem. Eng. Sci.*, **42**, 2667 (1987).
Smoglie, C., and J. Reimann, "Two-phase Flow Through Small Branches in a Horizontal Pipe with Stratified Flow," **12**, 609 (1986).
Sun, B., "Simulations of Gas-Liquid and Gas-Solid Two-phase Flows," PhD Thesis, Illinois Inst. of Technol., Chicago (1996).

Manuscript received Sept. 16, 1996, and revision received Feb. 26, 1997.